

## Supporting Information

### Deformation of Soft Particles with controlled elasticity by Liquid-Liquid Interfacial Tension

Benedikt Sapotta<sup>a,b</sup>, Jongmin Q. Kim<sup>a</sup>, Norbert Willenbacher<sup>b</sup> and Siyoung Q. Choi<sup>a†</sup>

- <sup>a</sup> Department of Chemical and Biomolecular Engineering, Korea Advanced Institute of Science and Technology (KAIST), Daejeon, South Korea.  
<sup>b</sup> Faculty of Chemical and Process Engineering, Karlsruhe Institute of Technology (KIT), Karlsruhe, Germany.  
<sup>†</sup> Authors to whom correspondence should be addressed.  
E-Mail: [sqchoi@kaist.ac.kr](mailto:sqchoi@kaist.ac.kr)

#### Soft Particle Preparation

To prepare soft particles, we thoroughly mixed base and curing agent in a 1.5 mL reaction tube and filled the resulting PDMS resin into a glass beaker. In the next step, we added deionised water with the mass ratio water:base:curing agent specified at 100:10:1. Subsequently, a PDMS resin in water emulsion was prepared by homogenization at 8000 rpm for 3 min with a Polytron PT 1300 D homogenizer (Kinematica, Switzerland) which was immediately placed into a heated bath afterwards. The curing temperature was set to 40 °C with the temperature controlling thermocouple being placed inside the emulsion. To reduce the effect of temperature gradients, both the emulsion and the heated bath were stirred at 80 rpm. At designated time intervals, emulsion samples were pipetted into a 1.5 mL reaction tube and placed into an iced bath to achieve thermal quenching. The samples remained inside the iced bath until the deformation experiment, which was carried out within less than 4 h following the particle preparation step.

#### SEM-sample preparation

To prepare the SEM-samples, soft PDMS particles were deformed at the interface between water and 3M Novec 7500 Engineered Fluid and subsequently cured at 40°C overnight. In the next step, most of the water phase was removed from the deformation bath. As the air/water-interfacial tension is larger than the sum of the oil/water- and oil/air-interfacial tension, the remaining water droplet submerged into the oil phase. The interface between the water droplet and the oil phase is jammed with deformed particles and the droplet can easily be picked and placed on the SEM-holder. Let water evaporate.

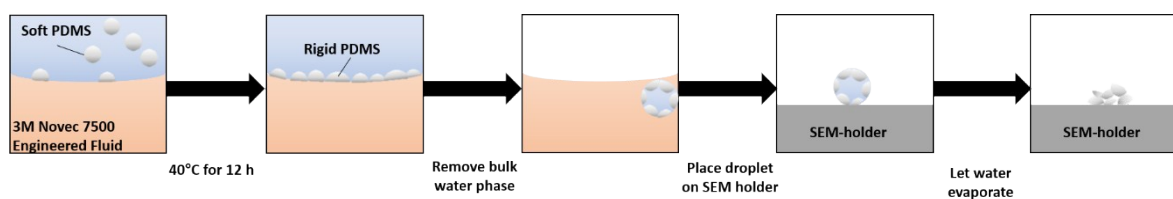


**Fig. S1:** Schematic depiction of SEM-sample preparation

**Characterization of Sylgard 184 prior to the curing reaction**

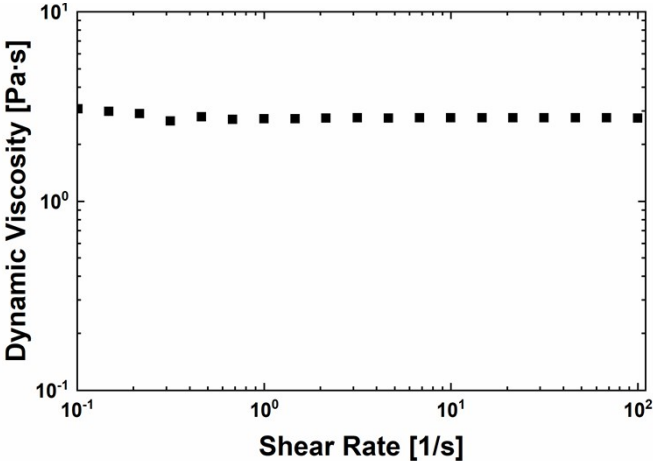


**Fig. S2:** Dynamic viscosity of Sylgard 184 directly after mixing base and curing agent (10:1) as a function of the shear rate at 25°C. The viscosity is not a function of the shear rate thus the PDMS resin behaves as a Newtonian liquid.

**Frequency sweep**

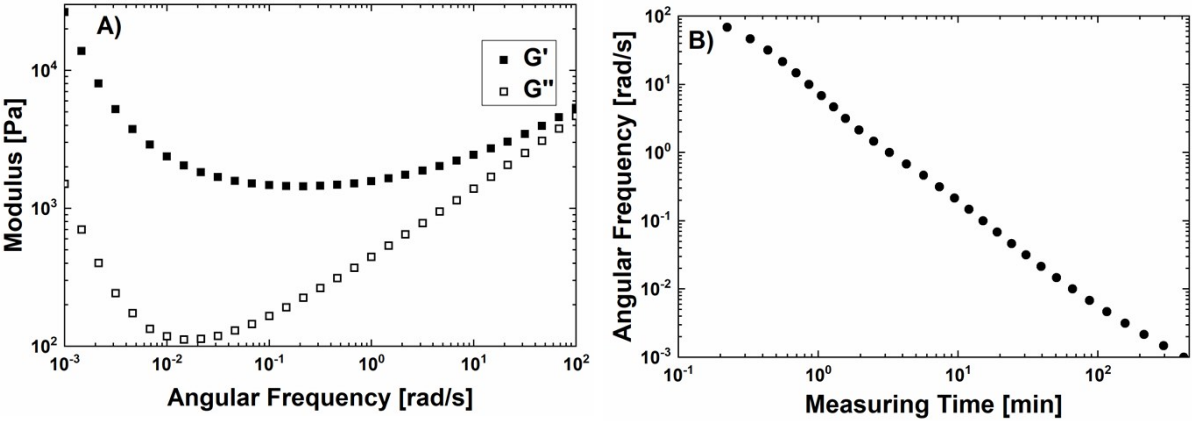


**Fig. S3:** **A)** Frequency sweep of Sylgard 184 recorded at 25 °C after having cured for 180 min at 40°C, same as Fig. 2B). **B)** Accumulated measuring time during the frequency sweep. The measurement was carried out by gradually reducing the applied angular frequency  $\omega$  starting at  $\omega = 100$  rad/s. The smaller  $\omega$ , the longer the required measuring time. The curing reaction continues at room temperature and causes the moduli to increase at prolonged measuring times thereby interfering with the actual frequency sweep.

### Creep and recovery test to assess plastic deformation

In order to gain a better understanding when and to what extent our model material is subject to plastic deformation, we conducted a creep and recovery test. For this purpose, we tracked the shear strain response of our sample when applying and later removing a constant shear stress. As sample we used Sylgard 184 at the same curing state as the previous frequency sweep i.e. after having cured at 40°C for 180 min. The shear stress was applied for 170 s followed by a 280 s recovery period. In total, we successively investigated four different shear stresses with the resulting graphs displayed in Fig S4.

Except for the largest shear stress, the sample deforms largely reversibly with the retardation time ranging between 0.2 - 0.5 s. For these three cases, we observe a total strain recovery of 96 % during the designated recovery period. This means that plastic deformation is, at most, responsible for only 4 % of the recorded shear strain response. Note, that the continuing curing reaction prevents us from determining the actual residual strain which can only be determined for prolonged recovery periods. In the case of the largest shear stress examined at 10 000 Pa, the sample starts to yield causing irreversible, plastic deformation which is clearly visible during the recovery period.

Based on the creep measurements, the relatively large degree of deformation in the second regime may in part be explained by the occurrence of plastic deformation. This would be supported by the fact that we could only observe second regime deformation at the curing time closest to the actual crossover point. It cannot be ruled out that particles cured for 180 min will deform even beyond the determined apparent equilibrium size at prolonged timescales, especially if the stress exerted on the particles by the o-w interface exceeds the particle yield point. Unfortunately, the occurrence of internal flow in the deformation bath did not allow us to keep track of individual particles for long periods of time. However, given that particle stretching at the o-w interface in the second regime significantly slows down to the point that it appears to terminate within a few seconds (see movie S1), we believe that the initial particle response upon contact with the interface is primarily of elastic nature. Therefore, we consider the application of the concept of elastocapillarity on the second regime deformation in Fig. 4 to be appropriate. As the data shown in Fig. S4 proves that our model material is able to tolerate a large amount of elastic strain while retaining its solid-like behaviour we are convinced that plastic deformation is negligible for the third, fourth and fifth regime.

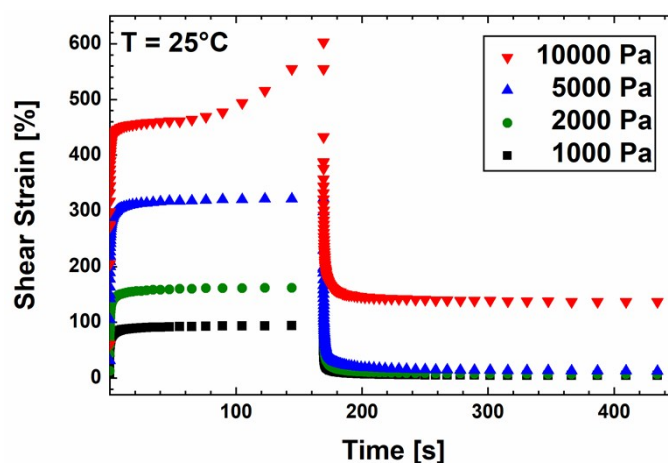


**Fig. S4:** Creep and recovery test of Sylgard 184 after having cured for 180 min at 40°C. The data was collected by tracking the shear strain response when applying a constant shear stress which was removed after 170 s. Sylgard 184 is highly deformable tolerating elastic shear strains of up to 300 %. Note, that the shear strain measured at the rheometer cannot be directly equated with the degree of deformation determined at the deformation bath. The yield point at the present curing state appears to be between 5000 and 10 000 Pa.

## Light Microscope and Spectral Data of the Light Source

We used a Thorlabs 30 mm cage system with its main components displayed in Fig. S5. The typical spectral data of our light source is shown in Fig. S6.

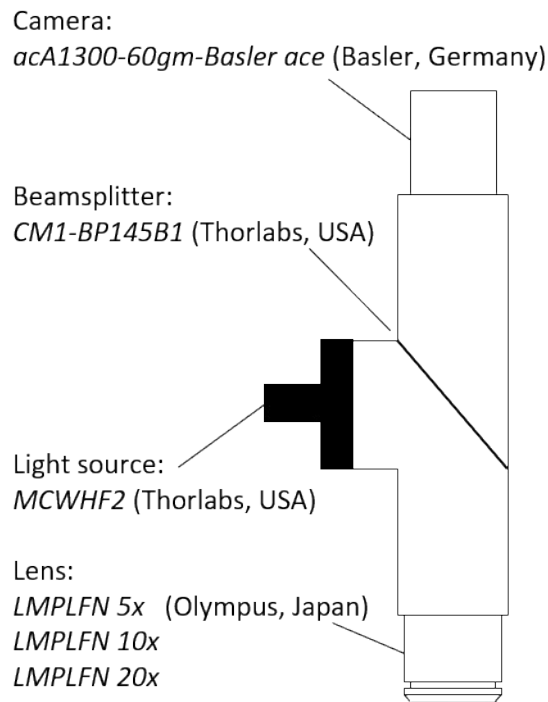


Fig. S5 Light Microscopy System used to record particle deformation at the deformation bath.

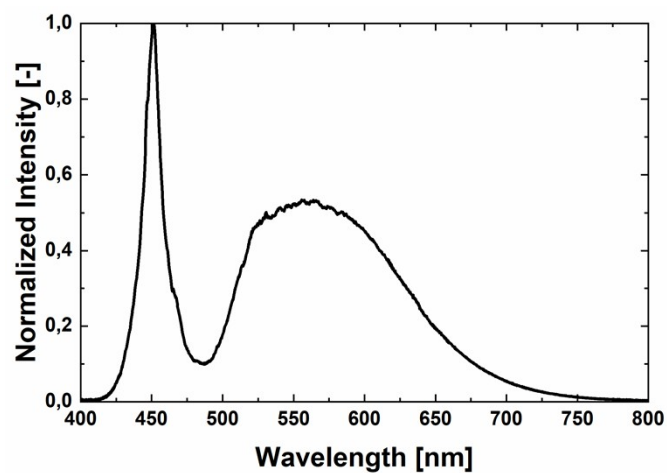
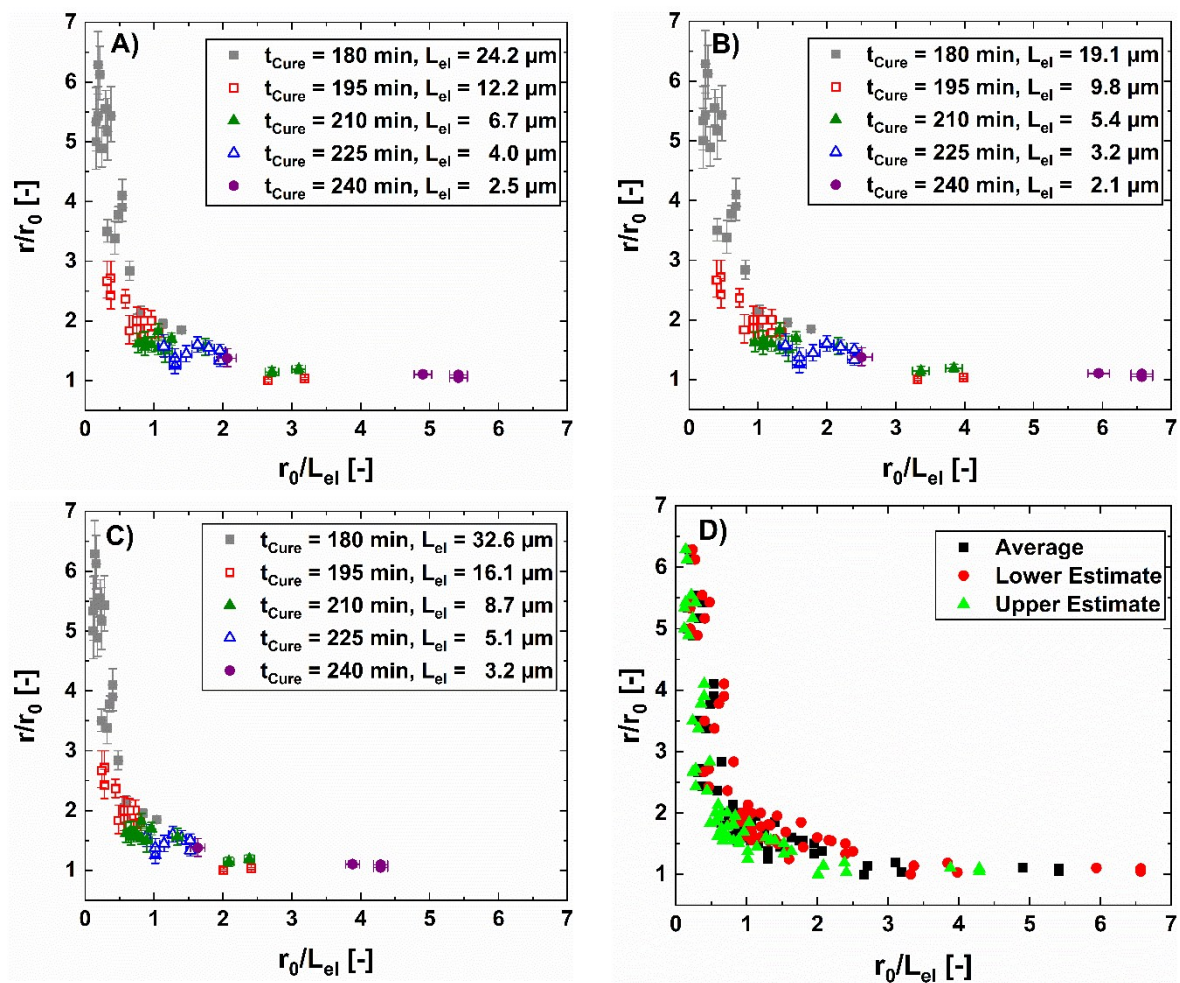


Fig. S6 Typical spectral data of the *MCWHF2* LED-lamp. Data provided by Thorlabs.<sup>1</sup>

#### Error estimate for Fig. 4:

The individual, known error sources are outlined in Table S1. Their effect on Fig. 4 is summarized in Fig. S7.

Table S1: Summary of error sources	
$\gamma_{o/w}$	The interfacial tension between 3M Novec 7500 Engineered Fluid and water was measured with the pendant drop method. The averaged value for $\gamma_{o/w}$ was 43.5 mN/m with an uncertainty of $\pm 0.5$ mN/m. Due to scarcity in reported values we could not compare $\gamma_{o/w}$ with literature values.
$G'$ $G''$	The storage and loss moduli of Sylgard 184 were determined with the MCR 302 rheometer (Anton Paar, Austria). The curing graph shown in Fig. 2 shows the average value together with the standard deviation based on five individual measurements.
$r_0$ $r$	The apparent particle radius before and after deformation were extracted from the microscopy videos taken at our deformation bath. The uncertainty in particle radius is assumed to be one pixel.



**Fig. S7** Error estimate for Fig. 4. The graph is subject to a random error (inaccuracy in image processing) and a systematic error (uncertainty of the elastocapillary length  $L_{el}$ ). The uncertainty of  $L_{el}$  is caused by the measurement inaccuracy of the storage modulus and the interfacial tension. Fig. 4 was drawn with the averaged  $L_{el}$  and is shown in **A)**, **B)** and **C)** represent the same graph with the upper and lower estimate for  $L_{el}$  instead. **D)** shows the averaged, lower estimate and upper estimate of  $L_{el}$  combined in one graph. While the error in  $L_{el}$  might cause the data points to shift horizontally, it does not obstruct the validity of Fig. 4 as a whole and its classification into the second, third and fourth

regime.

## **Movies**

Movie S1: Second regime deformation  
Movie S2: Third regime deformation  
Movie S3: Fourth regime deformation

## **References**

1. *Thorlabs, typical spectral data for MCWHF2. Data retrieved from [https://www.thorlabs.de/newgroupage9.cfm?objectgroup\\_id=5206&pn=MCWHF2](https://www.thorlabs.de/newgroupage9.cfm?objectgroup_id=5206&pn=MCWHF2) on April 22nd, 2019.*